Understanding Miltefosine-Membrane Interactions Using Molecular Dynamics Simulations

Matheus Malta de Sá‡, Vishnu Sresht‡, Carlota Oliveira Rangel-Yagui*, and Daniel Blankschtein*.

‡These authors contributed equally.

*Carlota Oliveira Rangel-Yagui
E-mail: corangel@usp.br

*Daniel Blankschtein
E-mail: dblank@mit.edu

Supplementary Material

The MARTINI force field

The MARTINI force field (version 2.0), developed by Marrink and co-workers[1], was used in this work to model lipids, cholesterol, water, and miltefosine. In this force field, each coarse-grained (CG) particle consists of approximately 4 heavy atoms. Each interaction site falls into one of the four main categories: polar (P), nonpolar (N), apolar (C), and charged (Q). In order to allow for a more accurate representation, each particle is, in turn, assigned a number to indicate its degree of polarity (from 1, representing low polarity, to 5, representing high polarity). The subtypes are also classified according to their ability to establish hydrogen-bonding (*d* = donor, *a* = acceptor, *da* = donor and acceptor, and 0 = none).

The non-bonded interactions are modeled according to the Lennard-Jones (LJ) 12-6 potential, as follows:

$$U_{LJ}(r) = 4\epsilon_{ij}\left[\left(\frac{\sigma_{ij}}{r}\right)^{12} - \left(\frac{\sigma_{ij}}{r}\right)^{6}\right] \quad \text{(S1)}$$

where σ_{ij} is the closest distance r between two particles, and ϵ_{ij} is the strength of this interaction. The same effective size σ = 0.47 nm is assumed for each interaction pair, with the exception of rings (σ = 0.43 nm), antifreeze particles (σ = 0.57 nm), and interactions between charged (Q-type) and apolar (C_1 and C_2 types) particles (σ = 0.62 nm).

In addition, charged particles interact via shifted Coulombic potential as follows:

$$U_{el}(r) = \frac{q_i q_j}{4\pi\epsilon_0\epsilon_r r} \quad \text{(S2)}$$

where q the charge of the particle at the distance r, and ϵ is the relative permittivity.

Bonds are modeled using a weak harmonic potential:

$$V_{bond}(r) = \frac{1}{2}K_{bond}(r - r_{bond})^2 \quad \text{(S3)}$$

where $r_{bond} = \sigma$, and K_{bond} = 1250 kJ mol^{-1} nm^{-2}.

A weak harmonic potential is also used to model angles:

$$V_{angle}(\theta) = \frac{1}{2} K_{angle} [cos(\theta) - cos(\theta_0)]^2 \quad \text{(S4)}$$

where K_{angle} = 25 kJ mol^{-1}, and θ_0 = 180° for aliphatic chains.

In order to prevent out-of-plane distortions in more complicated geometries, an improper dihedral angle potential is modelled as follows:

$$V_{id}(\theta) = K_{id}(\theta - \theta_{id})^2 \quad \text{(S5)}$$

where θ is the angle between the planes containing atoms i, j, k and j, k, l, and θ_{id} is the equilibrium angle between these planes, with force constant K_{id}.

Miltefosine Parametrization

Coarse-Grained Representation

Milfosine (MIL) parameters are not part of the original MARTINI force field.[1] However, the force-field building blocks allow for the coarse-grained (CG) representations of generic molecules to be extended if chemical characteristics, such as polarity and charge distribution, of the constitutive moieties are known. In this work, the bonded interactions for MIL and the particle types were chosen by chemical analogy with dodecylphosphocholine (DPC), a standard component of the MARTINI force field (Tables S1 A, B, and C). The four-to-one mapping was maintained, and one extra C1 particle was added in relation to the DPC structure to appropriately represent MIL (Figure S1).

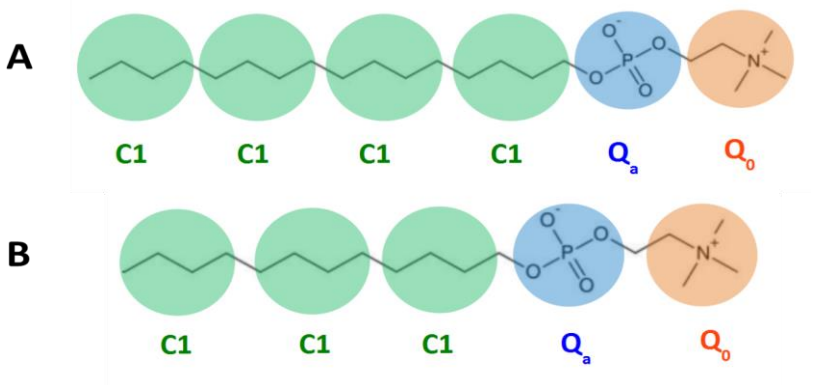

Figure S1: Miltefosine (MIL) (A) and docecylphosphocholine (DPC) (B) structures mapped according to the MARTINI force field bead types: Q_0: positively-charged type; Q_a: negatively-charged type; C1: apolar type.

Table S1: Parameters for the coarse-grained representation of miltefosine.

A

Atom number	MARTINI particle type	Charge	Building block
1	Q_0	+1.0	NC3
2	Q_a	-1.0	PO4
3	C1	0.0	C4
4	C1	0.0	C4
5	C1	0.0	C4
6	C1	0.0	C4

B

Bonds *i,j*	Length (nm)	K_{bond} (kJ mol^{-1} nm^{-2})
1,2	0.47	1250
2,3	0.47	1250
3,4	0.47	1250
4,5	0.47	1250
5,6	0.47	1250

C

Angle *i,j,k*	Angle (deg)	K_{angle} (kJ mol^{-1} rad^{-2})
3,4,5	180	25
4,5,6	180	25

Model Validation

GROMACS 4.5.5[2] was utilized for our CG simulation of MIL with the standard MARTINI water molecule (W) and time step of 20 fs. The cut-offs for nonbonded interactions (Lennard-Jones and Coulomb) were the same as those used to simulate the bilayers. Water and MIL were coupled separately to a Berendsen thermostat[3] maintained at a temperature of 323 K, with τ_T = 0.3 ps. An isotropic Berendsen barostat[3] was used to maintain the pressure of the simulation box at 1 bar, with τ_P = 3.0 ps. The system was simulated for 100 ns. The functions utilized to model the stretching, bending, and dihedral were identical to those used in the standard MARTINI force field.

The chosen CG parameters were compared to atomistic (AA) simulations of MIL. For the AA simulation, MIL was modeled with the force-field parameters developed by Berger et al.[4] The molecule was placed in a cubic box, 1 nm away from the box's edge, solvated with simple-point charge (SPC) water molecules.[5] Lennard-Jones and Coulomb interactions were cut off at 1.2 nm, and the Particle-Mesh Ewald (PME) method was used to compute long-range electrostatic interactions.[6,7] The LINCS algorithm[8] was used to constrain bond lengths, permitting a 2 fs time step. Before running the actual MD simulations, the system was equilibrated using position-restrained MD as follows: i) 1 ns of isochoric-isothermal (NVT) equilibration at 323K using the Berendsen thermostat, with τ_T = 0.3, and ii) 1 ns isothermal-isobaric (NPT) at 1 bar, using the Berendsen barostat with τ_P = 3.0 ps. After these two equilibration steps, the system was simulated for 100 ns without any restraints, at 323 K using the V-rescale thermostat,[9] with τ_T = 0.3, and isotropic pressure coupling with the Parrinello-Rahman barostat[10] with τ_P = 1.0 ps to keep pressure at 1 bar.

The CG bonded parameters were validated comparing the angle and dihedral distribution for the CG beads 1, 2, 3 and 4 to the distribution obtained from the AA simulation of the center of mass of the corresponding groups.

Figure S2 shows that there is excellent agreement between the CG and the AA angle and dihedral distributions. Therefore, we consider the selected bonded parameters for MIL to be appropriate to represent this molecule.

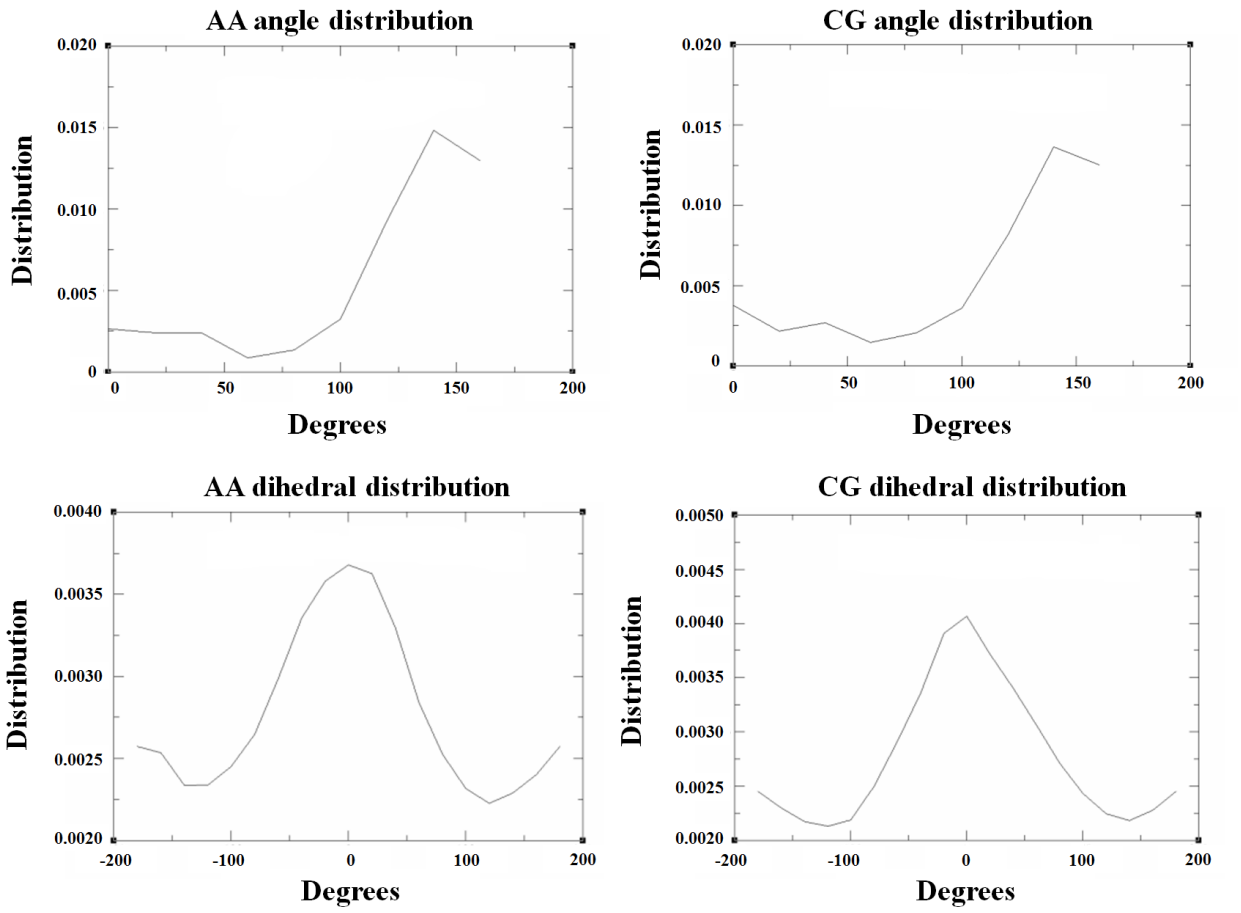

Figure S2. Dihedral and angle distributions for the atomistic (AA) and the coarse-grained (CG) MIL simulations.

Summary of Bilayer Self-Assembly Simulations

Figure S3 shows the temporal evolution of the mean surface area per lipid obtained from our simulations for the DPPC bilayer, whose experimentally determined mean surface area/lipid is 0.64 nm². The lack of significant variation of this value seen in Figure S3 supports our assertion that these bilayers were sufficiently stable during our simulations.

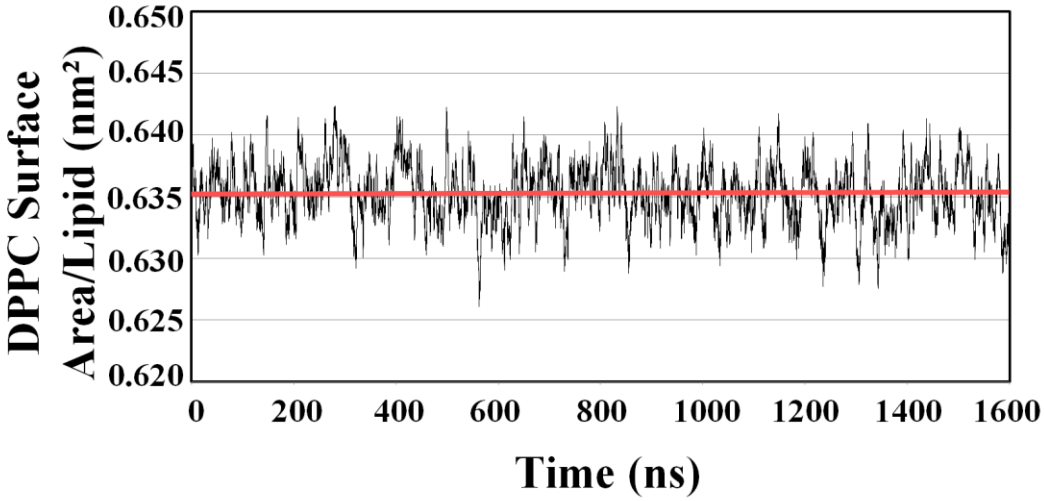

Figure S3. Temporal evolution of the DPPC surface area/lipid. The red line represents the mean value of the DPPC surface area/lipid, which is equal to 0.635 nm². For DAPC, DUPC, and bilayers containing 10% and 30% of CHOL, experimental data are not available.

Table S2 provides a summary of the statistics of all the bilayers simulated in this study, including a comparison of the mean surface area per lipid obtained from our simulations with the corresponding values obtained from experimental observations.

Table S2: Summary of the self-assembly simulations.

Bilayer composition	Total number of lipids (half the number per leaflet)	Absolute temperature (phase transition temperature) [K][a]	t [ns]	Mean surface area/lipid[a] [nm^2][b]	Bilayer thickness [nm]
DPPC	512	323 (314)	1600	0.64 (0.63 at 323 K)	4.17
DOPC	512	300 (253)	1600	0.75 (0.72 at 303 K)	4.56
POPC	512	300 (271)	1600	0.64 (0.64 at 303 K)	4.34
DAPC	512	300 (203)	1600	0.86	3.86
DUPC	512	300 (220)	1600	0.75	3.63
DPPC:CHOL (10%)	456:48	323	3600	0.58	4.24
DPPC:CHOL (30%)	342:144	323	3600	0.47	4.43

[a]Available experimental values of the phase transition temperatures,[11] and the surface areas/lipid[12] are shown in parenthesis.

[b]Mean value of the surface area/lipid measured for the duration of the simulation. In order to assure the calculations were done in a stabilized system, the first half of the simulations was not included in this evaluation.

Effects of Miltefosine on Bilayer Organization

Order Parameter of the Lipid Tails

We studied the effects of MIL on bilayer organization at local and bilayer-wide length scales by measuring the order parameter of the lipids acyl chains in the upper and lower leaflets of each bilayer, with and without MIL, respectively. The order parameter is given by:

$$S_2 = \langle {}^1\!/_2\,(3cos^2\theta_n - 1)\rangle \qquad \text{(S6)}$$

where θ_n is the angle between the vector connecting the $(n-1)$ and the $(n+1)$ sites of the hydrocarbon chain and the bilayer normal, z. The $\langle\ \rangle$ brackets indicate that the given value is an average over all lipids, while ignoring any cholesterol that may be present in the bilayer, during the simulation. The sites used to calculate θ_n are indicated in Figure S4.

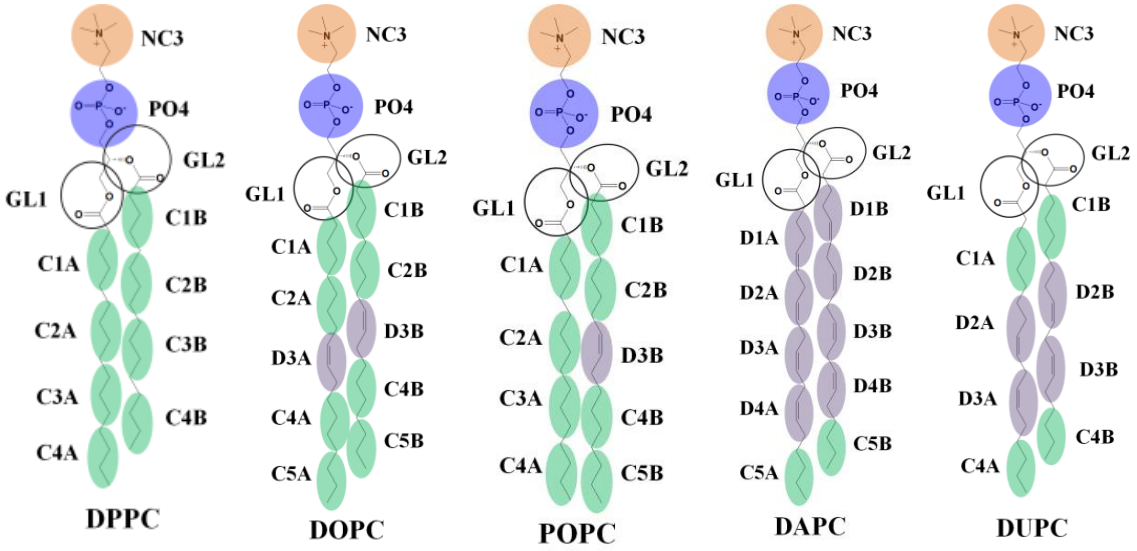

Figure S4. Sites used to calculate the angle θ_n for the order parameter, S_2. The bead types are the same as those used in the MARTINI force field. NC3 is the choline group; PO4 is the phosphate group; GL1 and GL2 are glycerol groups; the groups starting with C (C1-C5) correspond to saturated moieties; the groups starting with D (D1-D4) correspond to unsaturated moieties.

Miltefosine has a very small bilayer-wide effect on the order parameter S_2 of the tails of bilayer-forming lipids, as can be seen in Figure S5. Here, we compared the difference in the order parameter averaged over the upper leaflet (containing Miltefosine) and the lower leaflet

(without Miltefosine). The *p*-values shown in Figure S5 correspond to the hypothesis that the S_2 order parameters of the lipid tails in the upper and the lower leaflets arise from the same distribution of order parameters (by one-tailed Welsh's test).

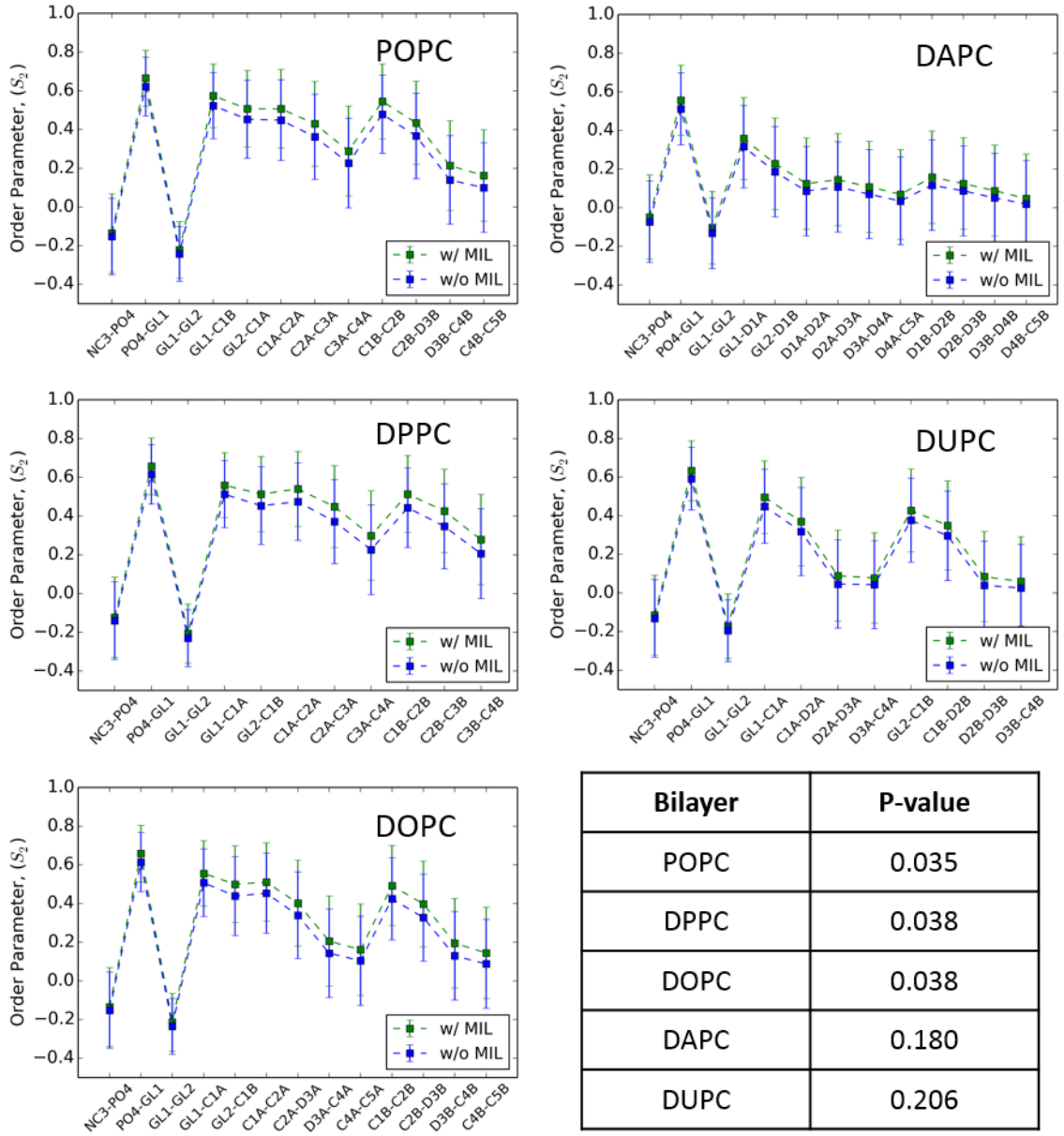

Bilayer	P-value
POPC	0.035
DPPC	0.038
DOPC	0.038
DAPC	0.180
DUPC	0.206

Figure S5. The presence of Miltefosine (green line) has a statistically insignificant effect on polyunstaturated lipid bilayers (DAPC and DUPC), but leads to a very slight increase in the order parameter in bilayers composed of more saturated lipids (POPC, DPPC, and DOPC).

Interestingly, the distance of a lipid molecule from MIL is completely uncorrelated to its order parameter, as can be seen in Figure S6.

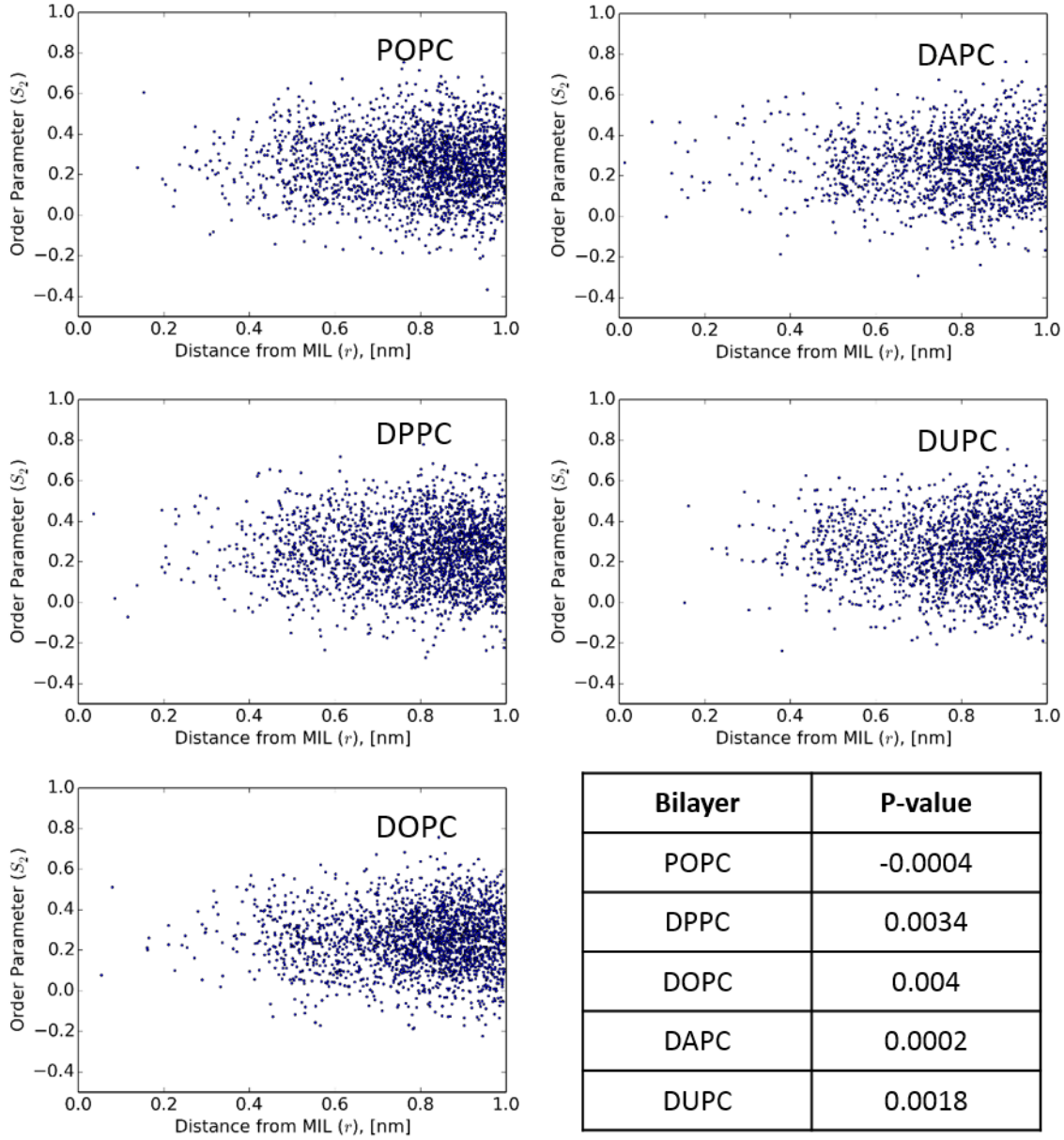

Bilayer	P-value
POPC	-0.0004
DPPC	0.0034
DOPC	0.004
DAPC	0.0002
DUPC	0.0018

Figure S6. Overall order parameter versus distance of a lipid molecule from MIL. The table of R-values shows that both quantities are uncorrelated.

Identification of Ordered Domains by Voronoi Tesselation

We also verified the existence of domains and phase separation in the presence of MIL using a Voronoi tessellation map. The head groups in DPPC, DOPC, POPC, DAPC, and DUPC were selected as the center of the Voronoi polygons. The polygons were connected based on their coordination number, that is, the number of nearest neighbors surrounding one molecule. Here, we used a cutoff value of $N_{cut} = 6$ neighbors, because many researchers have modeled the packing of a cholesterol molecule and lipid acyl chains, as well as of liquid-ordered/liquid-disordered phase coexistence, as an hexagonal lattice.[13-15] The local area per lipid and coordination number were plotted as a function of distance of the polygon centers from MIL. This analysis was performed for both the upper and the lower bilayer leaflets, and the corresponding results for DPPC (saturated) and DUPC (poly-unsaturated) bilayers are shown in Figure S7.

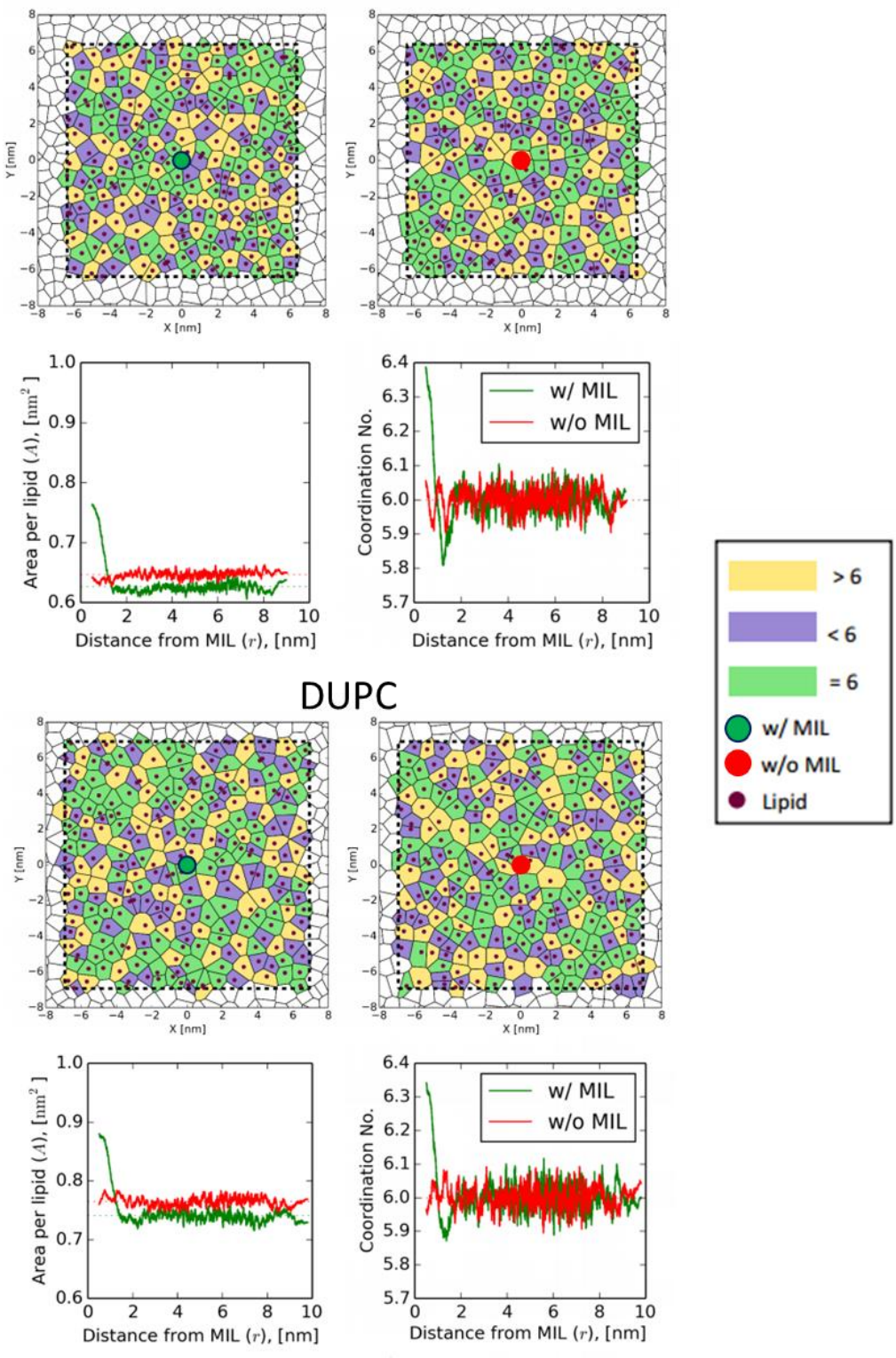

Figure S7. Voronoi tessellation maps and plots showing the variation of area per lipid and coordination number in the upper (with MIL) and the lower (without MIL) bilayer leaflets for both DPPC and DUPC.

The Voronoi tessellation maps confirm the findings from our studies on the effects of a miltefosine molecule on the order parameter of the lipids comprising the bilayer. Figure S7 shows that very close to the MIL molecule, there is a compression of lipid molecules leading to a lower area per lipid and a lower coordination number. However, at small to intermediate distances away from the MIL molecule, the area per lipid and the coordination number quickly reach the values observed for lipid molecules in the leaflet in the absence of MIL. Note that very close to the MIL molecule, the tessellation algorithm ignores the presence of MIL and ends up assigning a larger area to lipid molecules which are adjacent to the MIL molecule.

It is noteworthy that these results are different from those corresponding to the classical model of a surfactant interacting with lipids forming a lamellar phase. In this model, in order to fit the lamellar packing, the molecular asymmetry of the single-chained surfactant must be compensated by lateral headgroup compression (dehydration) and lateral hydrocarbon chain expansion (fluidization), leading to a decrease in the order parameter.[16] However, our data corroborate the experimental findings that Miltefosine and Edelfosine do not change the biophysical state of lipid bilayers, and, at pharmacological concentrations, both drugs are unlikely to solubilize cellular membranes.[17]

Calculation of Permeance from (Umbrella) MD Simulations

In all the simulations performed in this study, we have assumed that the bilayer is homogenous in the lateral coordinates (i.e., in the *x*-*y* directions in Figure 1b of the main text). We shall, therefore, only consider the one-dimensional transport of MIL through a bilayer (denoted by *i*) along the *z* direction shown in Figure 1b of the main text.

If the transport is diffusion-controlled, then, the driving force for transport is the negative of the gradient of the chemical potential of MIL across bilayer *i*, $-\nabla\mu^{(i)}$.[18] The average velocity of MIL in bilayer *i*, $u^{(i)}$ is directly proportional to the driving force,[25] that is,

$$u^{(i)} = -\frac{1}{\xi^{(i)}}\nabla\mu^{(i)} \tag{S7}$$

where the proportionality constant, $1/\xi^{(i)}$, is the reciprocal of the friction coefficient of MIL in bilayer *i*, $\xi^{(i)}$. Einstein's kinetic theory connects the friction coefficient to the diffusion coefficient of MIL in bilayer *i*, $D^{(i)}$, as follows:[18]

$$D^{(i)} = \frac{RT}{\xi^{(i)}} \tag{S8}$$

The flux of MIL across a unit area of bilayer *i*, in the *z* direction, per unit time, $J^{(i)}$, in the diffusion controlled regime is given by:[18]

$$J^{(i)} = c^{(i)}u^{(i)} = -\frac{c^{(i)}D^{(i)}}{RT}\nabla\mu^{(i)} = -\frac{c^{(i)}(z)D^{(i)}(z)}{RT}\cdot\frac{d\mu^{(i)}(z)}{dz} \tag{S9}$$

where, in accordance with our assumption of homogeneity in the *x*-*y* directions, the gradient of the chemical potential has been replaced by its spatial derivative in the *z* direction.

If one is interested in the transport of MIL across bilayer *i* from position, z_1, to position z_2, and if there is no buildup of MIL at any intermediate position $z_1 < z < z_2$, then the flux $J^{(i)}(z)$ must be the same at all positions between z_1 and z_2. This, in turn, implies that $J^{(i)}(z)$ is a constant, and Eq. (S9) can be readily integrated as follows:

$$J^{(i)}\,RT\int_{z_1}^{z_2}\frac{1}{c^{(i)}(z)D^{(i)}(z)}dz=\int_{z_1}^{z_2}\frac{d\mu^{(i)}(z)}{dz} \tag{S10}$$

$$\Rightarrow J^{(i)}\,RT\int_{z_1}^{z_2}\frac{1}{c^{(i)}(z)D^{(i)}(z)}dz=\mu^{(i)}(z_2)-\mu^{(i)}(z_1) \tag{S11}$$

$$\Rightarrow J^{(i)}\frac{RT}{c_0}\int_{z_1}^{z_2}\frac{c_0/c^{(i)}(z)}{D^{(i)}(z)}dz=\mu^{(i)}(z_2)-\mu^{(i)}(z_1) \tag{S12}$$

where $c_0 = c^{(i)}(z_1)$ is the concentration of MIL in bilayer i at $z = z_1$. Given a fixed difference in MIL chemical potentials, $\mu^{(i)}(z_2)-\mu^{(i)}(z_1)=\Delta\mu$, the transport of MIL across bilayer i is therefore characterized solely by the permeance, $P^{(i)}$, defined as:

$$\frac{1}{P^{(i)}}=\int_{z_1}^{z_2}\frac{c_0/c^{(i)}(z)}{D^{(i)}(z)}dz \tag{S13}$$

Using Eq. (S13) in Eq. (S12) yields:

$$J^{(i)}=P^{(i)}\cdot\frac{c_0}{RT}\,\Delta\mu \tag{S14}$$

Equation (S14) shows that P_i is a measure of how fast MIL moves from z_1 to z_2 in bilayer i, for a given concentration of MIL on one side of the bilayer, c_0, and having assumed that the chemical potential difference, $\mu^{(i)}(z_2)$ - $\mu^{(i)}(z_1) = \Delta\mu$, is constant. Equation (S14) also shows that the relative rate of movement of MIL through bilayers 1 and 2, $J^{(1)}/J^{(2)}$ is equal to the ratio of their permeances, $P^{(1)}/P^{(2)}$, to MIL.

The expression for the permeance can be simplified by assuming that, at equilibrium, MIL obeys Boltzmann statistics, namely, that the concentration of MIL in bilayer i, $c^{(i)}(z)$, is proportional to the exponential of the potential of mean force of a MIL molecule, $\exp(-\Phi^{(i)}(z)/k_BT)$. Taken together with the definition that $c_0 = c^{(i)}(z_1)$, this implies that:

$$\frac{c^{(i)}(z)}{c_0}=\exp\left[-\frac{\Phi^{(i)}(z)-\Phi^{(i)}(z_1)}{k_BT}\right]=exp\left[-\Delta\Phi^{(i)}(z)\right] \tag{S15}$$

Using this result in Eq. (S13), we obtain an expression for the permeance of bilayer i in terms of the potential of mean force experienced by MIL and its diffusion coefficient in bilayer i.

$$\Rightarrow \frac{1}{P^{(i)}} = \int_{z_1}^{z_2} \frac{\exp \Delta\Phi^{(i)}(z)}{D^{(i)}(z)} \, dz \qquad \text{(S16)}$$

Because the potential of mean force was already computed using Umbrella Sampling MD simulations, Eq. (S16) states that we only need to estimate the diffusion coefficient, $D^{(i)}$ (z), at various depths in the bilayer in order to calculate the permeance, $P^{(i)}$.

The work of Woolf and Roux[19] and Hummer[20] on the estimation of the diffusion coefficient from non-equilibrium MD simulations leads to the following expression for the diffusion coefficient:

$$D^{(i)}(z = \langle z \rangle) = \mathrm{Var}(z)/\tau_z \qquad \text{(S17)}$$

where ⟨z⟩ is the average of z during a biased simulation, Var (z) is the variance, and τ_z is the characteristic autocorrelation time. The characteristic autocorrelation time is calculated as follows:[20]

$$\tau_z = \frac{\int_0^\infty \langle \Delta z(t) \Delta z(0) \rangle dt}{\mathrm{Var}(z)} \qquad \text{(S18)}$$

Using Eq. (S18) in Eq. (S17), we arrive at the final expression for $D^{(i)}$:

$$D^{(i)}(z = \langle z \rangle) = \frac{\mathrm{Var}(z)^2}{\int_0^\infty \langle \Delta z(t) \Delta z(0) \rangle dt} \qquad \text{(S19)}$$

An example of the autocorrelation function ⟨Δz(t)Δz(0)⟩ obtained from a single biased (umbrella) MD simulation is shown in Figure S8.

The Permeance values obtained using this theory for the different bilayers considered in this study are reported in Table S3. For each bilayer i, $P_1^{(i)}$ was defined as the MIL permeance between the exterior of the lipid bilayer and the equilibrium position in one of the bilayer leaflets. In this case, z_1 corresponds to bulk water and z_2 corresponds to the equilibrium position in one of the leaflets. $P_1^{(i)}$ is therefore a quantitative measure of the rate at which MIL enters lipid bilayer i from bulk water. In addition, $P_2^{(i)}$ corresponds to the MIL permeance between the equilibrium positions in the two leaflets of bilayer i. In this case, z_1 corresponds to the equilibrium position in one leaflet and z_2 corresponds to the equilibrium position in the second

leaflet. $P_2^{(i)}$ is therefore a quantitative measure of the rate at which MIL flip-flops between the two bilayer leaflets

Table S3. Miltefosine permeance values, P_1 and P_2, for the bilayers considered.

Bilayer	$\boldsymbol{P_1}$ **(m/s)**	$\boldsymbol{P_2}$ **(m/s)**
DPPC + 0% cholesterol	0.381	7.64×10^{-3}
DPPC + 10% cholesterol	0.210	3.94×10^{-3}
DPPC + 30% cholesterol	0.685	1.10×10^{-7}
DAPC	0.649	N/A*
DOPC	0.267	4.65×10^{-6}
DUPC	0.681	2.28×10^{-2}
POPC	0.379	1.44×10^{-4}

*For bilayers consisting of lipids like DAPC, there is only a single central, equilibrium position, and, therefore, no value for P_2.

Autocorrelation Functions from (Umbrella) MD Simulations

In the system studied here, the autocorrelation function ACF(Δt) is a measure of the average correlation between the position of a miltefosine molecule at $x(t)$ and its position after a time difference, Δt (with the average taken over all times t for the duration of the simulation trajectory). For a molecule in vacuum which does not experience any friction, the autocorrelation function is expected to be very large, because the molecule will move in a straight line with x varying monotically with time t. On the other hand, if the molecule undergoes pure Brownian motion, the variation of its position, x, will be random, ensuring that the autocorrelation function is zero for all Δt. In the system studied here, the miltefosine molecule is driven by the potential of mean force while under the influence of a non-zero frictional resistance. Consequently, the ACF is large for small values of Δt, and then decays to zero as Δt tends to ∞, where the autocorrelation time, τ_z, is a measure of how fast the ACF decays to zero (Figure S8).

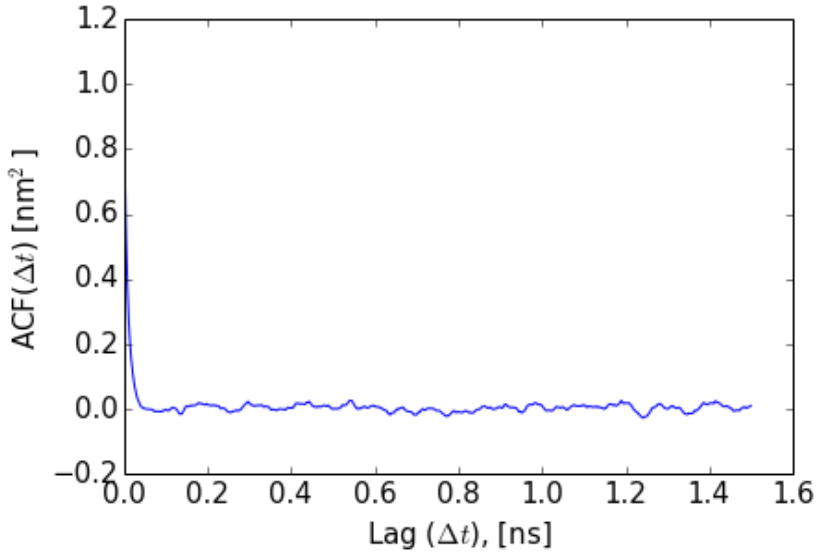

Figure S8. The autocorrelation time, τ_z, is a measure of how fast the autocorrelation function decays to zero. Here, τ_z decays rapidly to zero as Δt becomes larger.

Diffusivity of MIL in Lipid Bilayers Calculated from Umbrella Sampling Simulations

The diffusivities $D(z)$ of MIL in the bilayers was calculated as a function of the distance of MIL above the bilayer center (shown relative to the bulk diffusivity D_{bulk} of MIL in water in Figure S9). These diffusivities were used to calculate the permeance of MIL through the bilayer.

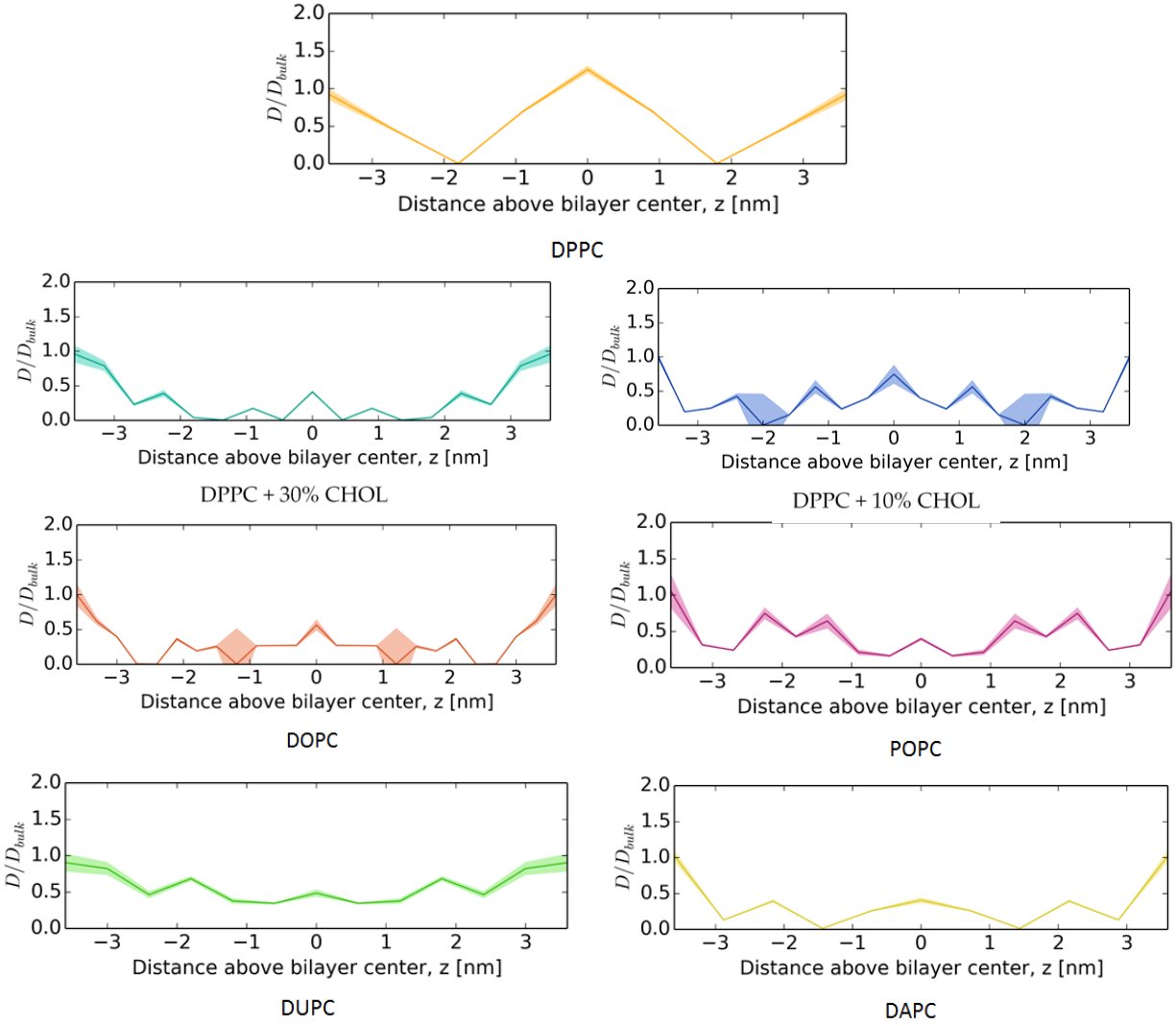

Figure S9. The diffusivity of MIL, D, in the bilayers simulated in this study relative to the bulk diffusivity, D_{bulk}, of MIL in water (3.4×10^{-10} m^2/s). The shaded regions represent the 1 standard deviation error in D.

Radial Distribution Functions of CHOL in DPPC Bilayers

The radial distribution functions quantifying the spatial organization of cholesterol molecules around other cholesterol molecules in bilayers of DPPC with 10% and 30% cholesterol are shown in Figure S10a. The smaller primary peak (at 0.5 nm) indicates that there is a lower probability of finding CHOL molecules at this distance, suggesting stronger intermolecular repulsions resulting from the insufficient screening of the electrostatic interactions between cholesterol molecules at these cholesterol concentrations. This intermolecular repulsion is consistent with observations of the instability of cholesterol clusters.[21,22] This conclusion is confirmed by the PMF curve between two CHOL molecules (Figure S10b), where the ΔG corresponding to the minimum at 0.5 nm is about +0.8 k_BT in a DPPC bilayer containing 30% CHOL.

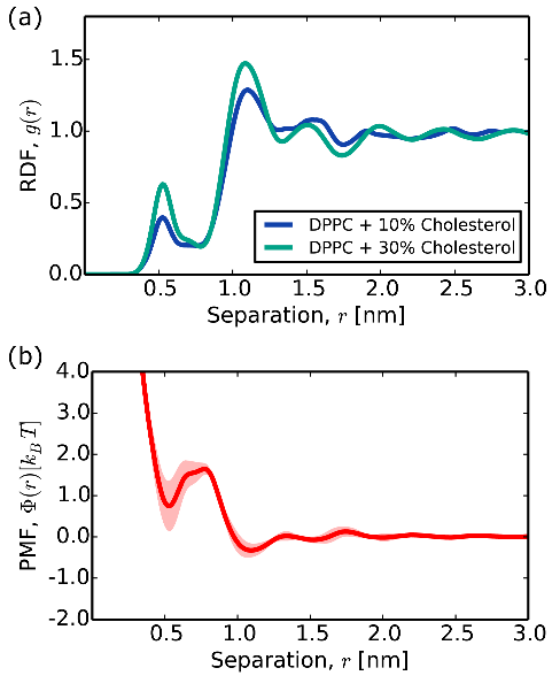

Figure S10. The Radial Distribution Function (RDF) between the 'C2' beads in the MARTINI representation of cholesterol is shown in **(a)**, and the PMF between cholesterol molecules as derived from the RDF is shown in **(b)**.

References

1. Marrink, S. J.; Risselada, H. J.; Yefimov, S.; Tieleman, D. P.; de Vries, A. H. The MARTINI force field: coarse grained model for biomolecular simulations. *J. Phys. Chem. B*. **2007**, 111, 7812-7824.

2. Hess, Berk, et al. "GROMACS 4: Algorithms for highly efficient, load-balanced, and scalable molecular simulation." *J. Chem. Theory and Comput*. **2008**, *4*, 435-447.

3. Berendsen, H. J. C.; Postma, J. P. M.; van Gunsteren, W. F.; DiNola, A.; Haak, J. R. Molecular dynamics with coupling to an external bath. *J. Chem. Phys*. **1984**, 81, 3684-3690.

4. Berger, O.; Edholm, O.; Jähnig, F. Molecular dynamics simulations of a fluid bilayer of dipalmitoylphosphatidylcholine at full hydration, constant pressure, and constant temperature. *Biophys. J*. **1997**, 72, 2002-2013.

5. Berendsen, H. J. C.; Postma, J. P. M.; van Gunsteren, W. F.; Hermans, J. In *Intermolecular Forces*; Pulman, B., Ed.; D. Reidel: Dordrecht, The Netherlands, 1981; pp 331-342.

6. Darden, T.; York, D.; Pedersen, L. Particle mesh Ewald: An N-log(N) method for Ewald sums in large systems. *J. Chem. Phys*. **1993**, 98, 10089-10092.

7. Essmann, U.; Perera, L.; Bekowitz, M. L.; Darden, T.; Lee, H.; Pedersen, L. G. A smooth particle mesh Ewald method. *J. Chem. Phys*. **1995**, 103, 8577-8593.

8. Hess, B.; Bekker, H.; Berendsen, H. J. C.; Fraaije, J. G. E. M. LINCS: A linear constraint solver for molecular simulations. *J. Comput. Chem*. **1997**, 18, 1463-1472.

9. Bussi, F.; Donadio, D.; Parrinello, M. Canonical sampling through velocity rescaling. *J. Chem. Phys*. **2007**, 126, 014101.

10. Parrinello, M.; Rahman, A. Polymorphic transitions in single crystals: A new molecular dynamics method. *J. Appl. Phys*. **1981**, 52, 7182-7190.

11. Silvius, J. R. In Thermotropic Phase Transitions of Pure Lipids in Model Membranes and Their Modifications by Membrane Proteins; Jost, P. C.; Griffith, O. H., Eds.; John Wiley & Sons, Inc., New York, **1982**; pp 239-281.

12. Kučerka, N.; Nieh, M. P.; Katsaras, J. Fluid phase lipid areas and bilayer thicknesses of commonly used phosphatidylcholines as a function of temperature. *Biochim. Biophys. Acta* **2011**, *1808*, 2761-2771.

13. Chong, P. L. Evidence for regular distribution of sterols in liquid crystalline phosphatidylcholine bilayers. *Proc. Natl. Acad. Sci*. **1994**, 91, 10069-10073.

14. Sodt, A. J.; Sandar, M. L.; Gawrisch, K.; Pastor, R. W.; Lyman E. The molecular structure of the liquid-ordered phase of lipid bilayers. *J. Am. Chem. Soc*. **2014**, 136, 725-732.

15. Virtanen J. A.; Ruonala, M.; Vauhkonen, M.; Somerharju P. Lateral organization of liquid-crystalline cholesterol-dimyristoylphosphatidylcholine bilayers. Evidence for domains with hexagonal and centered rectangular cholesterol superlattices. *Biochemistry*. **1995**, 34, 11568-11581.

16. Heerklotz, H.; Binder, H.; Lantzsch, G.; Klose, G. Lipid/Detergent Interaction Thermodynamics as a Function of Molecular Shape. *J. Phys. Chem. B*. **1997**, 101, 639-645.

17. Castro, B. M.; Fedorov, A.; Hornillos, V.; Delgado, J.; Acuña, A. U.; Mollinedo, F.; Prieto, M. Edelfosine and miltefosine effects on lipid raft properties: membrane biophysics in cell death by antitumor lipids. *J. Phys. Chem. B*. **2013**, 117, 7929-7940.

18. Bird, R. Byron, Warren E. Stewart, and Edwin N. Lightfoot. *Transport phenomena*. John Wiley & Sons, New York, **2007**.

19. Woolf, T. B.; & Roux, B. Conformational Flexibility of *o*-Phosphorylcholine and o-Phosphorylethanolamine: A Molecular Dynamics Study of Solvation Effects. *J. Am. Chem. Soc.* **1994,** *116*, 5916–5926.

20. Hummer, G. Position-Dependent Diffusion Coefficients and Free Energies from Bayesian Analysis of Equilibrium and Replica Molecular Dynamics Simulations. *New J. Phys.* **2005,** *7*, 34–34.

21. Dai, J.; Alwarawrah, M.; Huang, J. Instability of cholesterol clusters in lipid bilayers and the cholesterol's Umbrella effect. *J. Phys. Chem. B*. **2010,** *114*, 840–848.

22. Waheed, Q.; Tjörnhammar, R.; Edholm, O. Phase transitions in coarse-grained lipid bilayers containing cholesterol by molecular dynamics simulations. *Biophys. J*. **2012,** *103*, 2125–2133.